The scalar feed

Special reprint
from
AEÜ ARCHIV FÜR ELEKTRONIK UND ÜBERTRAGUNGSTECHNIK
ELECTRONICS AND COMMUNICATION
Band 26 (1972), pp. 22–30

The Scalar Feed

by JOZEF K. M. JANSEN, MARTIN E. J. JEUKEN and CEES W. LAMBRECHTSE

The Scalar Feed

by JOZEF K. M. JANSEN, MARTIN E. J. JEUKEN and CEES W. LAMBRECHTSE *

The electromagnetic field in the grooves of a corrugated conical horn antenna has been investigated. The investigation starts by modifying the boundaries of the grooves in such a way that they coincide with the spherical coordinate system. Under the condition that the width of the grooves is small compared with the wavelength, the following results are obtained. The dominant mode in the grooves is a TM mode and the radiation pattern of the antenna is symmetrical with respect to the axis of the antenna, provided the depth of the grooves is a quarter of a wavelength and the right excitation has been applied. Experiments confirm the theory. The paper concludes with information concerning the design of the scalar feed.

Kegelhornantenne mit Rillen

Das elektromagnetische Feld in den Rillen einer Kegelhornantenne wird analysiert. Die Untersuchung beginnt mit der Anpassung der Wände der Rillen an ein Kugelkoordinatensystem. Unter der Voraussetzung, daß die Breite der Rillen klein gegen die Wellenlänge ist, werden folgende Ergebnisse gefunden: Die Grundwelle in den Rillen ist eine TM-Welle und die Strahlungscharakteristik der Antenne ist symmetrisch bezogen auf die Achse der Antenne, vorausgesetzt, daß die Tiefe der Rillen ein Viertel der Wellenlänge ist und die richtige Anregung angewendet wurde. Experimente bestätigen die Theorie. Der Beitrag schließt mit einer Betrachtung über den Entwurf von Kegelhornantennen mit Rillen.

1. Introduction

The illumination of a paraboloid reflector antenna depends on the properties of the feed used. In order to obtain a high efficiency it is necessary that the radiation pattern of the feed is as uniform as possible and produces little spillover energy. Besides, it is desirable that the radiation pattern of the feed is symmetrical. Finally, the feed should possess a well-defined phase centre. For some applications, for instance for an antenna for line-of-sight communications it is necessary that the feed possesses the above properties in a large frequency range. A feed having all these properties has been proposed by SIMMONS and KAY [1] and they called it "scalar feed". The scalar feed is a conical horn antenna with grooves, perpendicular to the wall of the horn. The flare angle of this feed can be small or large. The paper of SIMMONS and KAY gives only some experimental results without a theoretical explanation of the radiation pattern of the scalar feed. Moreover this paper does not contain useful design information concerning the scalar feed. This is mainly caused by the fact that a theoretical explanation of the radiation pattern of these feeds was not available at the moment of publication.

The investigation of the scalar feed is greatly facilitated by making a distinction between scalar feeds with a small and with a large flare angle. The radiation pattern of a scalar feed with small flare angle can be found by treating it as an open circular waveguide radiator and, if necessary, with a quadratic phase field distribution across the aperture. This has already been done by JEUKEN and KIKKERT [2]. They studied, both theoretically and experimentally, the radiation pattern of a conical horn antenna with small flare angle. The inner wall of the cone consisted of a corrugated boundary, composed of circumferential grooves. They found a good agreement between the experimental and theoretical radiation pattern for the frequency range where the depth of the grooves was approximately a quarter of a wavelength. In the paper [2] the effect of the corrugations has been described by means of an impedance boundary condition and the detailed behaviour of the electromagnetic fields in the grooves was not considered.

Especially the frequency-dependent behaviour of the electromagnetic field in the grooves has not been taken into account. Therefore it was not possible to find a theoretical explanation of the fact that the antenna has a symmetrical radiation pattern in a frequency range where the depth of the grooves is approximately a quarter of a wavelength. An explanation of this phenomenon can be found by considering a corrugated cylindrical waveguide with grooves perpendicular to the wall of the waveguide. Each groove can be considered as a short-circuited radial waveguide. The modes in a radial waveguide can be classified as TE-modes and TM-modes with respect to the z-axis which is perpendicular to the direction of propagation [3]. If the distance between the fins of a groove is smaller than half a wavelength then a TM-mode and the dominant mode can propagate in the radial waveguide. Owing to the excitation only the TM-mode is excited [4]

If the circular waveguide has a diameter which is large compared to the wavelength, then it can be proved that the depth of the grooves should be a quarter of a wavelength in order to obtain a symmetrical power radiation pattern [4]. Using the above model CLARRICOATS and SAHA [5] were able to calculate the power radiation pattern of an open

* Ir. J. K. M. JANSEN, c/o Department of Mathematics, Dr. M. E. J. JEUKEN and Ir. C. W. LAMBRECHTSE, c/o Department of Electrical Engineering, Technological University, Eindhoven, Netherlands.

circular corrugated waveguide as a function of frequency. It should be noted that their results apply also to corrugated conical horn antennas with small flare angle [6].

CLARRICOATS [7] formulated the boundary conditions which should be applied in a corrugated conical horn antenna with large flare angle. He assumed that the grooves were perpendicular to the axis of the antenna. However, no information is available concerning the question whether this model can also be used for corrugated conical horn antennas with wide flare angles and grooves perpendicular to the wall of the antenna [8].

Summarising, we may say that there is a need of a better understanding of the effect of the corrugation, especially for antennas with wide flare angle. Moreover, it is desirable to compute the radiation pattern of the scalar feed with large flare angle in order to obtain useful design information concerning this feed. It is the purpose of the present paper to provide this information.

2. The Electromagnetic Field in the Groove

The scalar feed is a conical horn antenna with grooves perpendicular to the wall of the horn (Fig.1).

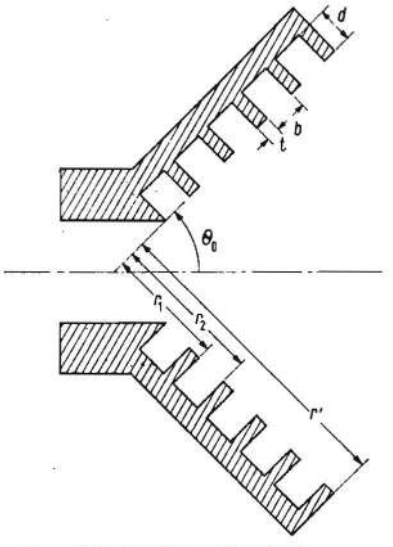

Fig. 1. The scalar feed.

The computation of the electromagnetic field in a groove is a difficult task, because the boundaries of the groove do not coincide with a coordinate system in which Maxwell's equations can be easily solved. Therefore, we change the boundaries of the groove in such a way that they coincide with the spherical coordinate system. For a groove not to close to the apex of the cone this is a good approximation.

One such groove is sketched in Fig. 2.

2.1. *The characteristic equation of the TM-mode*

In this section we shall study the conditions under which a TM-mode can propagate in a groove.

The TM-mode in the groove can be derived from the potential $A_r(r, \theta, \varphi)$ [9] by means of the following expressions

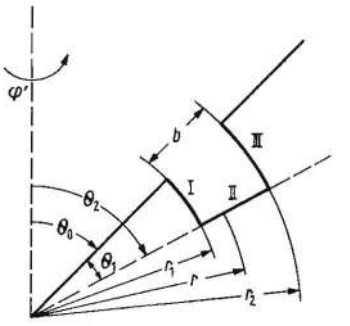

Fig. 2. Spherical groove and spherical coordinate system.

$$E_r = \frac{1}{\mathrm{j}\omega\varepsilon_0}\left(\frac{\partial^2}{\partial r^2} + k^2\right)A_r, \quad H_r = 0, \tag{1}$$

$$E_\theta = \frac{1}{\mathrm{j}\omega\varepsilon_0}\frac{1}{r}\frac{\partial^2 A_r}{\partial r\,\partial\theta}, \qquad H_\theta = \frac{1}{r\sin\theta}\frac{\partial A_r}{\partial\varphi},$$

$$E_\varphi = \frac{1}{\mathrm{j}\omega\varepsilon_0}\frac{1}{r\sin\theta}\frac{\partial^2 A_r}{\partial r\,\partial\varphi}, \qquad H_\varphi = -\frac{1}{r}\frac{\partial A_r}{\partial\theta}.$$

The function $A_r(r, \theta, \varphi)$ has the form

$$A_r(r,\theta,\varphi) = kr[a_n \mathrm{j}_n(kr) + b_n \mathrm{y}_n(kr)] \times \times [c_{nm}\mathrm{P}_n^m(\cos\theta) + d_{nm}\mathrm{Q}_n^m(\cos\theta)] \times \times (e_m\cos m\varphi + f_m\sin m\varphi). \tag{2}$$

In this expression the symbols used have the following meaning

$\mathrm{j}_n(kr)$, $\mathrm{y}_n(kr)$	are the spherical Bessel function and the spherical Neumann function, respectively.
$\mathrm{P}_n^m(\cos\theta)$, $\mathrm{Q}_n^m(\cos\theta)$	are the associated Legendre functions of the first kind and the second kind, respectively.
$a_n, b_n, c_{nm}, d_{nm}, e_m, f_m$	are constants which are determined by the boundary conditions and the strength of the electromagnetic field at the opening of the groove $\theta = \theta_0$.

The value of m depends on the way in which the electromagnetic field in the groove is excited. In most practical cases we have $m = 1$.

Application of the boundary condition $E_\varphi = 0$ for the boundaries I and III gives rise to the next equation (3)

$$\begin{vmatrix} \mathrm{j}_n(kr_1) + kr_1\mathrm{j}_n'(kr_1) & \mathrm{y}_n(kr_1) + kr_1\mathrm{y}_n'(kr_1) \\ \mathrm{j}_n(kr_2) + kr_2\mathrm{j}_n'(kr_2) & \mathrm{y}_n(kr_2) + kr_2\mathrm{y}_n'(kr_2) \end{vmatrix} = 0.$$

A special solution exists if $kb = \pi$; then $n = 0$. If there is a solution of eq. (3), then $A_r(r, \theta, \varphi)$ has the form (4)

$$A_r(r,\theta,\varphi) = kr\{[\mathrm{y}_n(kr_1) + kr_1\mathrm{y}_n'(kr_1)]\,\mathrm{j}_n(kr) - - [\mathrm{j}_n(kr_1) + kr_1\mathrm{j}_n'(kr_1)]\,\mathrm{y}_n(kr)\} \times \times [\mathrm{Q}_n^m(\cos\theta_2)\,\mathrm{P}_n^m(\cos\theta) - \mathrm{P}_n^m(\cos\theta_2)\,\mathrm{Q}_n^m(\cos\theta)] \times \times (e_m\cos m\varphi + f_m\sin m\varphi).$$

In the derivation of eq. (4) use has been made of the boundary conditions $E_\varphi = 0$ for $\theta = \theta_2$ and $E_r = 0$ for $\theta = \theta_2$.

We see that eq. (4) represents two independent solutions; one with $f_m = 0$ and the other with $e_m = 0$. Next, we assume that the width of the groove is small compared with the wavelength, so $kb \ll 1$. We apply the recurrence formulas [10]

$$f_n'(x) = \frac{n}{x} f_n(x) - f_{n+1}(x), \qquad f_n'(x) = f_{n-1}(x) - \frac{n+1}{x} f_n(x) \tag{5}$$

where $f_n(x)$ stands for $\mathrm{j}_n(x)$, $\mathrm{y}_n(x)$, respectively.

Next we define $kr_1 = x$, $kb = h$, and $kr_2 = x + h$. Using the expansions

$$\mathrm{j}_n(x+h) = \mathrm{j}_n(x) + h\,\mathrm{j}_n'(x) + 0(h^2),$$
$$\mathrm{y}_n(x+h) = \mathrm{y}_n(x) + h\,\mathrm{y}_n'(x) + 0(h^2)$$

in eq. (3) we obtain the equation

$$(-hx)\left[\frac{n(n+1)}{x} - x\right]\begin{vmatrix} \mathrm{j}_{n+1}(x) & \mathrm{y}_{n+1}(x) \\ \mathrm{j}_n(x) & \mathrm{y}_n(x) \end{vmatrix} = -\frac{h}{x^2}[n(n+1) - x^2] = 0. \tag{6}$$

So the solution of eq. (3) for small values of kb is given by

$$n(n+1) = (kr_1)^2 \tag{7}$$

or

$$n = -\frac{1}{2} \pm \left[\frac{1}{4} + (kr_1)^2\right]^{1/2}. \tag{8}$$

In the following considerations we shall omit the minus sign because it represents the same solution as the plus sign. From eq. (8) we now see that

$$n \approx kr_1 \quad \text{if} \quad kr_1 \gg 1 \quad \text{and} \quad kb \ll 1. \tag{9}$$

This result will be used in the following section. In conclusion, we see that a TM-mode can exist in the groove even if its width is small compared with the wavelength.

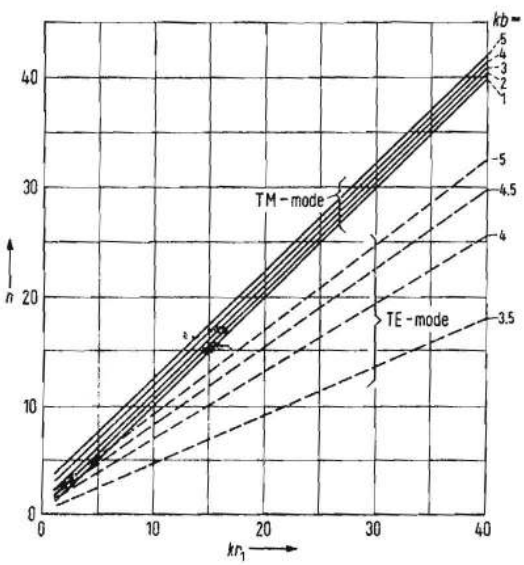

Fig. 3. n versus kr_1 with kb as parameter.

A numerical analysis of eq. (3), based on the method described in [11] gives n as a function of kr_1, for several values of kb. The results are collected in Fig. 3. Note that n is approximately a linear function of kr_1, which is in agreement with eq. (9).

A similar investigation can be carried out with the aim to find the conditions under which a TE-mode can propagate in a groove. The details of this investigation are given in [11]. The main conclusion is that a TE-mode cannot propagate in a groove, if the width of the groove is smaller than half a wavelength.

2.2. *The components of the electromagnetic field of the TM-mode*

From the preceding considerations we know that only a TM-mode can exist in the groove, provided the width of the groove is smaller than half a wavelength. So it is now interesting to investigate the components of the electromagnetic field of this mode in more detail.

In section 4 of the paper we shall prove that the boundary conditions $E_\varphi = 0$ and $Z_0 H_\varphi = 0$ give rise to a symmetrical radiation pattern. Therefore, we shall first investigate the conditions under which $Z_0 H_\varphi = 0$. From the general expression of A_r, eq. (4), we see that $Z_0 H_\varphi = 0$, if we can find a value of θ_0 which satisfies the equation (10)

$$\mathrm{P}_n^{m\prime}(\cos\theta_0)\,\mathrm{Q}_n^m(\cos\theta_2) - \mathrm{P}_n^m(\cos\theta_2)\,\mathrm{Q}_n^{m\prime}(\cos\theta_0) = 0$$

where the prime means differentiating with respect to the argument. Useful insight into the behaviour of the groove can be obtained if for the moment we restrict our considerations to the case that $kb \ll 1$ and $kr_1 \gg 1$. Then we know from eq. (9) that $n \gg 1$.

So an asymptotic expansion of $\mathrm{P}_n^m(\cos\theta)$ and $\mathrm{Q}_n^m(\cos\theta)$ can be substituted in eq. (10). These expansions are [12]

$$\mathrm{P}_n^m(\cos\theta) = \frac{\Gamma(m+n+1)}{\Gamma(n+3/2)}\left(\frac{\pi}{2}\sin\theta\right)^{-1/2} \times \cos\left[\left(n+\frac{1}{2}\right)\theta - \frac{\pi}{4} - \frac{m\pi}{2}\right] + 0\left(\frac{1}{n}\right), \tag{11}$$

$$\mathrm{Q}_n^m(\cos\theta) = \frac{\Gamma(m+n+1)}{\Gamma(n+3/2)}\left(\frac{\pi}{2\sin\theta}\right)^{1/2} \times \cos\left[\left(n+\frac{1}{2}\right)\theta + \frac{\pi}{4} + \frac{m\pi}{2}\right] + 0\left(\frac{1}{n}\right). \tag{12}$$

Substitution of eqs. (11) and (12) in eq. (10) and using the relation [13] (13)

$$L_n^{m\prime}(u) = \frac{-mu}{1-u^2} L_n^m(u) - \frac{1}{(1-u^2)^{1/2}} L_n^{m+1}(u)$$

where $L_n^m(u)$ stands for $\mathrm{P}_n^m(u)$ or $\mathrm{Q}_n^m(u)$, we find after several algebraical manipulations

$$\tan\left(n+\frac{1}{2}\right)(\theta_2 - \theta_0) = \tan\left(n+\frac{1}{2}\right)\theta_1 = (n+2)\tan\theta_0. \tag{14}$$

The solution of this equation is

$$\theta_1 = \frac{\arctan[(n+2)\tan\theta_0] + l\pi}{n + \frac{1}{2}}; \quad (15)$$

$$l = 0, 1, 2, \ldots$$

and for large values of n and θ_0 the approximation $\theta_1 \equiv \frac{\pi(2l+1)}{2n}$ is valid. We know that $n \approx kr_1$, so

$$\theta_1 = \frac{\pi(2l+1)}{2kr_1}. \quad (16)$$

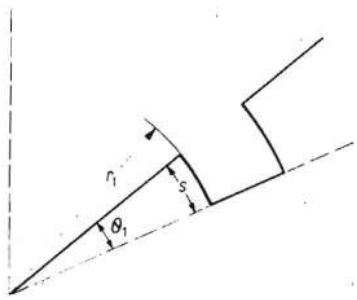

Fig. 4. Spherical groove with definition of s.

The depth of the groove s (Fig. 4) is now given by

$$s = r_1\theta_1 = \frac{\pi(2l+1)}{2k} = \frac{\lambda}{4}(2l+1) \quad (17)$$

and the important conclusion can be drawn that the depth of the groove should be the same for all grooves that are far enough from the apex of the cone.

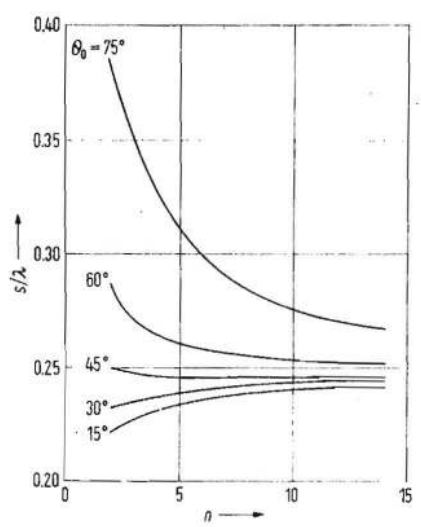

Fig. 5. s/λ versus n with flare angle θ_0 as parameter.

In the proof of eq. (17) we have assumed that the flare angle θ_0 is large enough. So there is need for an exact computation of the depth of the groove under the condition that $Z_0 H_\varphi = 0$ at the opening of the groove. Such a computation can be carried out starting from the Runge-Kutta method and is described in some detail in [11]. The results are given in Fig. 5 and we may draw the following conclusions:

i) for grooves for which $n > 15$, the depth of the grooves can be found using eq. (17);
ii) for grooves for which $5 < n < 15$, the depth of the grooves is virtually independent of θ_0 if $\theta_0 > 30°$;
iii) for grooves characterized by a low value of n and a low value of θ_0 we see that the depth of the grooves is a function of both n and θ_0.

So it is always possible to design the grooves in such a way that $Z_0 H_\varphi = 0$ at the opening of the grooves. Let us now study the electric field at the opening of the grooves. First we note that $E_\theta = 0$ if $Z_0 H_\varphi = 0$. For the case of $kb \ll 1$ some useful results can be derived from the general expressions (1) and (4). After a large amount of algebra we find

$$\frac{\mathrm{d}A_r}{\mathrm{d}(kr)} = \frac{(r-r_1)^2}{(kr_1)^2}[n(n+1) - (kr_1)^2]. \quad (18)$$

Using eqs. (1) and (6) we see that E_φ is zero in the groove. In the proof of eq. (18) use has been made of the same Taylor expansion, which has also been used in the derivation of eq. (6). This expansion is not valid for low values of kr_1. So, for grooves in the vicinity of the apex of the cone E_φ cannot be neglected.

However, extensive calculations, which are not included, show that $E_\varphi/E_r < 10^{-3}$ for $kr < 10$ and $kb \approx 1$.

2.3. *The boundary conditions at the wall of the corrugated horn*

The electromagnetic field at the opening of a narrow groove consists of the dominant TM-mode and evanescent modes. Experience teaches us that calculations concerning corrugated boundaries give useful results if the evanescent modes are neglected [14]. Suppose that there are many grooves per wavelength. Then we may formulate the boundary conditions at $\theta = \theta_0$ in terms of two impedances Z_φ and Z_r, defined by the relations

$$E_\varphi = Z_\varphi H_r, \quad E_r = Z_r H_\varphi. \quad (19)$$

We know that E_φ is zero at the opening of the grooves and at the dams, while currents in the φ-direction are possible. Hence $H_r \neq 0$ and $Z_\varphi = 0$. If we assume that the width of the dams is negligible, then we may write

$$Z_r = \frac{E_r}{H_\varphi} = -\frac{1}{\mathrm{j}\omega\varepsilon_0}\frac{n(n+1)}{r}A_r\left(\frac{\partial A_r}{\partial\theta}\right)^{-1} \quad (20)$$

with A_r given in eq. (4). Using $k^2r^2 \sim n(n+1)$ we find

$$Z_r = \frac{k^2 r}{\mathrm{j}\omega\varepsilon_0} \times \frac{Q_n^1(\cos\theta_2)\,P_n^1(\cos\theta_0) - P_n^1(\cos\theta_2)\,Q_n^1(\cos\theta_0)}{\sin\theta_0[Q_n^1(\cos\theta_2)\,P_n^{1\prime}(\cos\theta_0) - P_n^1(\cos\theta_2)\,Q_n^{1\prime}(\cos\theta_0)]} \quad (21)$$

Substitution of the expressions (11) and (12) in eq. (21) gives

$$Z_r \approx -\mathrm{j}Z_0\tan ks. \quad (22)$$

For the special case where the depth of the groove is a quarter of a wavelength we find $Z_r = \infty$.

3. The Electromagnetic Field in the Corrugated Conical Horn

Up till now we have studied the boundary conditions which should be applied at the boundary $\theta' = \theta_0$ for the calculation of the electromagnetic field in the region bounded by $\theta' < \theta_0$. Next we shall investigate which modes can exist in the corrugated horn. We observe that the boundary conditions can be satisfied with φ-independent TM-modes and TE-modes. However, these modes give rise to a dip in the radiation pattern in the forward direction and are not often used for antenna applications. In general, the electromagnetic field in the region $\theta' < \theta_0$ is a spherical hybrid mode. This mode can be understood as the sum of a TE-mode and a TM-mode. The components of this hybrid mode can be found from the potentials [9]

$$\begin{aligned} A_{r'}(r', \theta', \varphi') &= A_1 \mathrm{P}_\nu^1(\cos\theta') \cos\varphi' \hat{\mathrm{H}}_\nu^{(2)}(kr'), \\ F_{r'}(r', \theta', \varphi') &= A_2 \mathrm{P}_\nu^1(\cos\theta') \sin\varphi' \hat{\mathrm{H}}_\nu^{(2)}(kr') \end{aligned} \tag{23}$$

and summing the TE-part and TM-part. In eqs. (23) $\hat{\mathrm{H}}_\nu^{(2)}(kr')$ represents the spherical Hankel function of the second kind. It should be noted that primed coordinates are used for the description of the electromagnetic field in the horn. For the electromagnetic field in the grooves we have used unprimed coordinates. Finally, the coordinates of a point outside the horn antenna will be unprimed again. For the components of the spherical hybrid mode we now find

$$E_{r'} = \alpha(kr') \frac{\nu(\nu+1)}{\mathrm{j}kr'} \mathrm{P}_\nu^1(\cos\theta') \cos\varphi', \tag{24}$$

$$E_{\theta'} = \alpha(kr') \left[\frac{\mathrm{dP}_\nu^1(\cos\theta')}{\mathrm{d}\theta'} \xi_\nu(kr') - \delta \frac{\mathrm{P}_\nu^1(\cos\theta')}{\sin\theta'} \right] \cos\varphi', \tag{25}$$

$$E_{\varphi'} = \alpha(kr') \left[\frac{\mathrm{P}_\nu^1(\cos\theta')}{\sin\theta'} \xi_\nu(kr') + \delta \frac{\mathrm{dP}_\nu^1(\cos\theta')}{\mathrm{d}\theta'} \right] \sin\varphi', \tag{26}$$

$$Z_0 H_{r'} = \alpha(kr') \delta \frac{\nu(\nu+1)}{\mathrm{j}kr'} \mathrm{P}_\nu^1(\cos\theta') \sin\varphi', \tag{27}$$

$$Z_0 H_{\theta'} = \tag{28}$$

$$= \alpha(kr') \left[\delta \frac{\mathrm{dP}_\nu^1(\cos\theta')}{\mathrm{d}\theta'} \xi_\nu(kr') - \frac{\mathrm{P}_\nu^1(\cos\theta')}{\sin\theta'} \right] \sin\varphi',$$

$$Z_0 H_{\varphi'} = \tag{29}$$

$$= \alpha(kr') \left[\frac{\mathrm{dP}_\nu^1(\cos\theta')}{\mathrm{d}\theta} + \delta \xi_\nu(kr') \frac{\mathrm{P}_\nu^1(\cos\theta')}{\sin\theta} \right] \cos\varphi'$$

with the abbreviations

$$\begin{aligned} \alpha(kr') &= \frac{A_1 Z_0 \hat{\mathrm{H}}_\nu^{(2)}(kr')}{r'}, \\ \xi_\nu(kr') &= \frac{\mathrm{d}\hat{\mathrm{H}}_\nu^{(2)}(kr')}{\mathrm{j}k\,\mathrm{d}r'} \frac{1}{\hat{\mathrm{H}}_\nu^{(2)}(kr')}, \\ \delta &= A_2/A_1 Z_0 . \end{aligned} \tag{30}$$

In the expressions (24) to (29) the unknown quantities are δ and ν. Using the asymptotic expansion of $\hat{\mathrm{H}}_\nu^{(2)}(kr')$ we see that $\lim_{kr' \to \infty} \xi_\nu(kr') = -1$. For a point not too close to the apex of the cone we assume that $\xi_\nu(kr') \approx -1$.

The boundary condition $Z_\varphi = 0$ gives the relation

$$\frac{\mathrm{P}_\nu^1(\cos\theta)}{\sin\theta} + \delta \frac{\mathrm{dP}_\nu^1(\cos\theta)}{\mathrm{d}\theta}\bigg|_{\theta=\theta_0} = 0 . \tag{31}$$

The boundary condition $E_{r'} = Z_r H_{\varphi'}$ gives rise to the equation for ν

$$-\frac{\nu(\nu+1)}{\mathrm{j}kr'} \frac{Z_0}{Z_r} \mathrm{P}_\nu^1(\cos\theta) \frac{\mathrm{dP}_\nu^1(\cos\theta)}{\mathrm{d}\theta} - \left[\frac{\mathrm{dP}_\nu^1(\cos\theta)}{\mathrm{d}\theta} \right]^2 + \left[\frac{\mathrm{P}_\nu^1(\cos\theta)}{\sin\theta} \right]^2 \Bigg|_{\theta=\theta_0} = 0 . \tag{32}$$

This equation contains the variable r' which implies that ν is a function of r'. However, this is not possible because in eq. (23) the assumption has been made that the method of separation of variables can be applied. Hence eq. (32) can be solved only if we assume that $Z_r = \infty$. This assumption implies that the depth of the grooves is a quarter of a wavelength. It should be emphasised that up till now no solutions of Maxwell's equations for a corrugated conical horn with a boundary condition given by eqs. (19) and (21) has been found. For the special case $Z_r = \infty$ we find $A_2 = \pm Z_0 A_1$. So two classes of modes can propagated in the corrugated conical horn. The modes for which $A_2 = Z_0 A_1$ are called $HE_{1\nu}^{(1)}$-modes, while the other modes are $HE_{1\nu}^{(2)}$-modes.

Finally we find for the characteristic equation

$$\frac{\mathrm{dP}_\nu^1(\cos\theta')}{\mathrm{d}\theta'} \pm \frac{\mathrm{P}_\nu^1(\cos\theta')}{\sin\theta'}\bigg|_{\theta=\theta_0} = 0 . \tag{33}$$

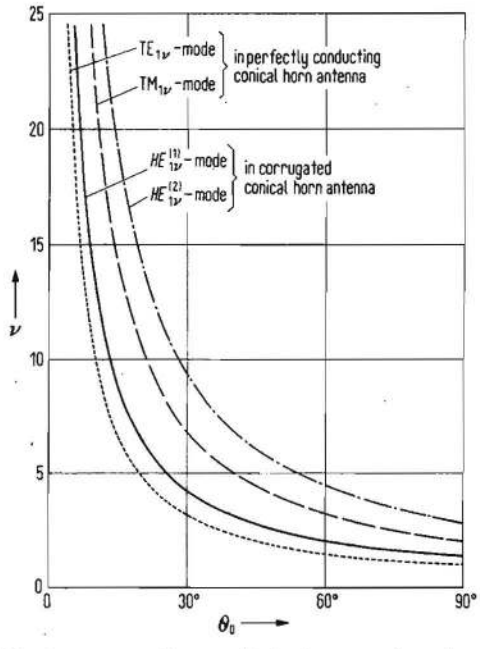

Fig. 6. ν versus flare angle θ_0 for several modes.

We have solved eq. (33) for the lowest value ν. The results are plotted in Fig. 6. For purposes of comparison we have also plotted the value of ν of the $TE_{1\nu}$-mode and the $TM_{1\nu}$-mode in a perfectly conducting conical horn. The function $\xi_\nu(kr')$ has also been computed for finite values of kr' and for those values of ν which occur for the $HE_{1\nu}^{(1)}$-mode in a very large horn and with flare angles $\theta_0 = 15°$, 30°, 45°, 60°, and 75°. The results are plotted in Fig. 7 and show that the approximation $\xi_\nu(kr') \approx -1$ is valid even for rather low values of kr'.

Let us now calculate the transverse electric and magnetic field components of the $HE_{1\nu}^{(1)}$-mode. Substitution of $A_1 Z_0 = A_2$ in eqs. (25), (26), (28), and (29) gives

$$E_{\theta'} = g_{1\nu}^{(1)}(r', \theta') \cos\varphi', \quad E_{\varphi'} = -g_{1\nu}^{(1)}(r', \theta') \sin\varphi',$$
$$Z_0 H_{\theta'} = -E_{\varphi'}, \qquad Z_0 H_{\varphi'} = E_{\theta'} \tag{34}$$

with $g_{1\nu}^{(1)}(r', \theta') = -\alpha(kr') f_{1\nu}^{(1)}(\theta')$,

$$f_{1\nu}^{(1)}(\theta') = \frac{\mathrm{d}P_\nu^1(\cos\theta')}{\mathrm{d}\theta'} + \frac{P_\nu^1(\cos\theta')}{\sin\theta'}.$$

Comparing eq. (33) with eq. (34) we see that all the transverse electric and magnetic components are zero for $\theta' = \theta_0$.

For the sake of completeness we also give the transverse electric and magnetic field components of the $HE_{1\nu}^{(2)}$-mode:

$$E_{\theta'} = g_{1\nu}^{(2)}(r', \theta') \cos\varphi', \quad E_{\varphi'} = g_{1\nu}^{(2)}(r', \theta') \sin\varphi',$$
$$Z_0 H_{\theta'} = -E_{\varphi'}, \qquad Z_0 H_{\varphi'} = E_{\theta'} \tag{35}$$

with $g_{1\nu}^{(2)}(r', \theta') = -\alpha(kr') f_{1\nu}^{(2)}(\theta')$,

$$f_{1\nu}^{(2)}(\theta') = \frac{\mathrm{d}P_\nu^1(\cos\theta')}{\mathrm{d}\theta'} - \frac{P_\nu^1(\cos\theta')}{\sin\theta'}.$$

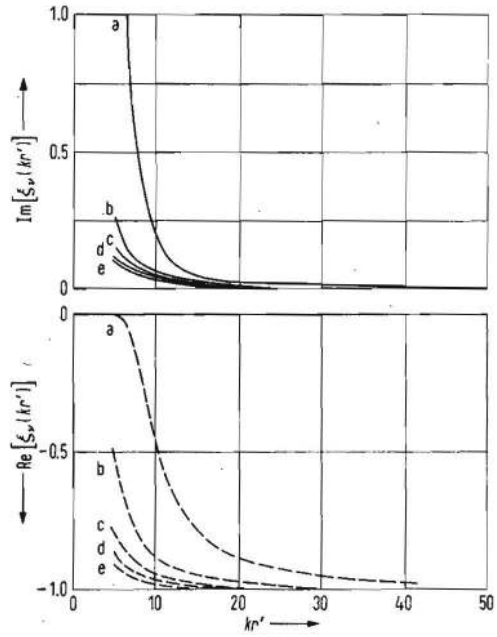

Fig. 7. $\mathrm{Re}[\xi_\nu(kr')]$ and $\mathrm{Im}[\xi_\nu(kr')]$ versus kr' with ν as parameter;
a) $\theta_0 = 15°$; $\nu = 8.74$,
b) $\theta_0 = 30°$; $\nu = 4.19$,
c) $\theta_0 = 45°$; $\nu = 2.71$,
d) $\theta_0 = 60°$; $\nu = 2.00$,
e) $\theta_0 = 75°$; $\nu = 1.59$.

4. The Radiation Pattern of the Corrugated Conical Horn Antenna

4.1. Computation of the radiation pattern

The electromagnetic field of a radiating conical horn antenna can be found from the following representation theorem [15]:

$$\underline{E}(\underline{r}) = \mathrm{curl}_p \int_{S_A} [\underline{n}' \times \underline{E}(\underline{r}')] G(\underline{r}, \underline{r}') \,\mathrm{d}S + \tag{36}$$
$$+ \frac{1}{\mathrm{j}\omega\varepsilon_0} \mathrm{curl}_p \,\mathrm{curl}_p \int_{S_A} [\underline{n}' \times \underline{H}(\underline{r}')] G(\underline{r}, \underline{r}') \,\mathrm{d}S,$$

$$\underline{H}(\underline{r}) = \mathrm{curl}_p \int_{S_A} [\underline{n}' \times \underline{H}(\underline{r}')] G(\underline{r}, \underline{r}') \,\mathrm{d}S - \tag{37}$$
$$- \frac{1}{\mathrm{j}\omega\mu_0} \mathrm{curl}_p \,\mathrm{curl}_p \int_{S_A} [\underline{n}' \times \underline{E}(\underline{r}')] G(\underline{r}, \underline{r}') \,\mathrm{d}S$$

with $G(\underline{r}, \underline{r}') = \frac{1}{4\pi} \frac{\mathrm{e}^{-\mathrm{j}k|\underline{r}-\underline{r}'|}}{|\underline{r}-\underline{r}'|}$.

In these expressions we have assumed that the outside of the horn antenna is perfectly conducting and no currents flow on the outside of the antenna. The aperture S_A is part of a sphere with radius r' (Fig. 8).

The far field approximation gives

$$E_\theta(r, \theta, \varphi) = \frac{\mathrm{e}^{-\mathrm{j}kr}}{r} \frac{\mathrm{j}k}{4\pi} \int_{S_A} [(E_{\varphi'} \cos\theta' - Z_0 H_{\theta'} \cos\theta) \sin(\varphi - \varphi') + (E_{\theta'} + Z_0 H_{\varphi'} \cos\theta' \cos\theta) \cos(\varphi - \varphi') +$$
$$+ Z_0 H_{\varphi'} \sin\theta \sin\theta'] \exp\{\mathrm{j}kr' [\cos\theta \cos\theta' + \sin\theta \sin\theta' \cos(\varphi - \varphi')]\} (r')^2 \sin\theta' \,\mathrm{d}\theta' \,\mathrm{d}\varphi', \tag{38}$$

$$E_\varphi(r, \theta, \varphi) = \frac{\mathrm{e}^{-\mathrm{j}kr}}{r} \frac{\mathrm{j}k}{4\pi} \int_{S_A} [-(E_{\theta'} \cos\theta + Z_0 H_{\varphi'} \cos\theta') \sin(\varphi - \varphi') + (-Z_0 H_{\theta'} +$$
$$+ E_{\varphi'} \cos\theta' \cos\theta) \cos(\varphi - \varphi') + E_{\varphi'} \sin\theta \sin\theta'] \exp\{\mathrm{j}kr' [\cos\theta \cos\theta' + \tag{39}$$
$$+ \sin\theta \sin\theta' \cos(\varphi - \varphi')]\} (r')^2 \sin\theta \,\mathrm{d}\theta' \,\mathrm{d}\varphi'.$$

Substituting eq. (34) in eqs. (38) and (39) and usings the relation

$$\exp[\mathrm{j}kr' \sin\theta \sin\theta' \cos(\varphi - \varphi')] = J_0(kr' \sin\theta \sin\theta') + \sum_{n=1}^{\infty} 2\,\mathrm{j}^n J_n(kr' \sin\theta \sin\theta') \cos n(\varphi - \varphi') \tag{40}$$

we obtain

$$E_\theta = -\frac{\mathrm{j}k}{4}\frac{\mathrm{e}^{-\mathrm{j}kr}}{r} A_1 Z_0 \frac{\hat{\mathrm{H}}_\nu^{(2)}(kr')}{r'} (r')^2 \cos\varphi\, F(\theta, \theta_0, kr'), \tag{41}$$

$$E_\varphi = \frac{\mathrm{j}k}{4}\frac{\mathrm{e}^{-\mathrm{j}kr}}{r} A_1 Z_0 \frac{\hat{\mathrm{H}}_\nu^{(2)}(kr')}{r'} (r')^2 \sin\varphi\, F(\theta, \theta_0, kr') \tag{42}$$

with

$$F(\theta, \theta_0, kr') = \int_0^{\theta_0} \{(\cos\theta + \cos\theta')[\mathrm{J}_0(kr'\sin\theta\sin\theta') + \mathrm{J}_2(kr'\sin\theta\sin\theta')] + (1 + \cos\theta\cos\theta') \times$$
$$\times [\mathrm{J}_0(kr'\sin\theta\sin\theta') - \mathrm{J}_2(kr'\sin\theta\sin\theta')] + 2\mathrm{j}\sin\theta\sin\theta'\,\mathrm{J}_1(kr'\sin\theta\sin\theta')\} \times \tag{43}$$
$$\times f_{1\nu}^{(1)}(\theta')\exp(\mathrm{j}kr'\cos\theta\cos\theta')\sin\theta'\,\mathrm{d}\theta'.$$

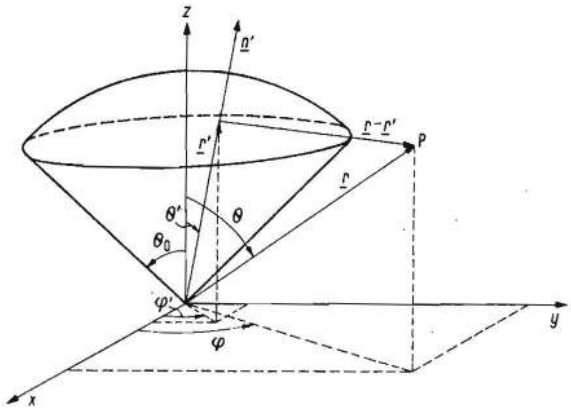

Fig. 8. Conical horn antenna with coordinate system.

From the eqs. (41) and (42) we derive that $|E_\theta|^2 + |E_\varphi|^2$ is independent of φ. It should be noted that the same result has already been found in [2] for the case that the flare angle was small. So the radiation pattern of a corrugated conical horn antenna is symmetrical, provided the depth of the grooves is a quarter of a wavelength, because in that case $Z_r = \infty$.

Substitution of eq. (35) in eqs. (38) and (39) shows that the $HE_{1\nu}^{(2)}$-mode has also a symmetrical radiation pattern, but with a dip for $\theta = 0$. This type of radiation pattern is not studied in this paper. From eqs. (41) and (42) we derive that (44)

$$\left|\frac{E_\theta(\theta, \theta_0 kr')}{E_\theta(0, \theta_0 kr')}\right| = \left|\frac{E_\varphi(\theta, \theta_0, kr')}{E_\varphi(0, \theta_0, kr')}\right| = \left|\frac{F(\theta, \theta_0, kr')}{F(0, \theta_0, kr')}\right|.$$

The function

$$20^{10}\log\left|\frac{F(\theta, \theta_0, kr')}{F(0, \theta_0, kr')}\right|$$

has been calculated for several values of θ_0 and kr'. From these calculations the beamwidth has been derived as a function of kr' for $\theta_0 = 15°$, 30°, 45°, 60°, and 75°. The results are collected in [11]. Some results are plotted in Figs. 9 and 10. It should be noted that these results are found under the assumption that the function $\xi_r(kr') = -1$ and under the assumption that $E_{\varphi'} = 0$ and $Z_0 H_{\varphi'} = 0$ at the boundary $\theta' = \theta_0$.

4.2. *Experimental investigation of the corrugated conical horn antenna*

4.2.1. λ/4-grooves

A comparison of the theory of Section 4.1 with experimental results is possible, provided the depth of the grooves is a quarter of a wavelength, because only in that case the boundary condition $Z_0 H_{\varphi'} = 0$ is satisfied. For that purpose several antennas have been constructed in such a way that a wide variation in both the flare angle θ_0 and the length r' of the antennas was obtained. All the grooves were of the same depth and this was a quarter of a wavelength at the frequency 14 GHz [11].

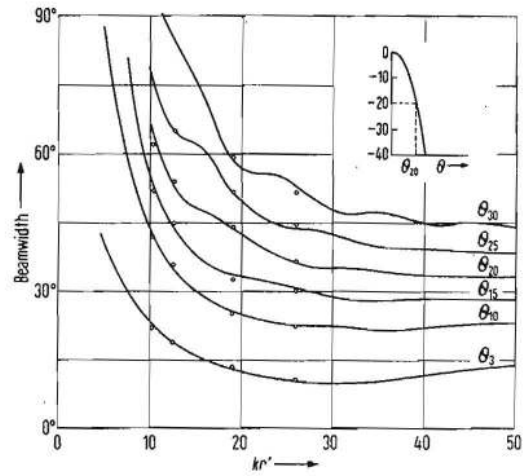

Fig. 9. Beamwidth versus kr' for $\theta_0 = 30°$; dots indicate experimental results obtained with several antennas at a frequency of 14 GHz.

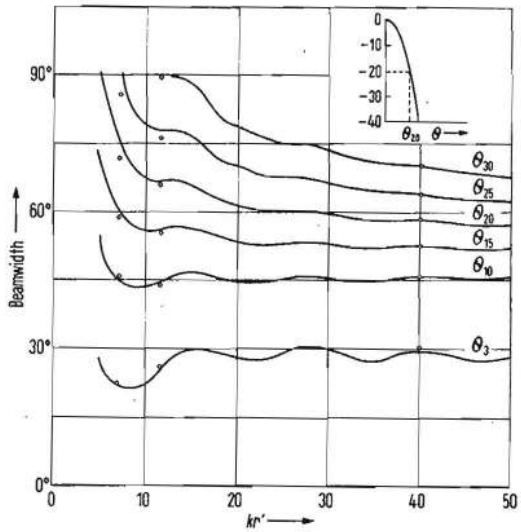

Fig. 10. Beamwidth versus kr' for $\theta_0 = 60°$; dots indicate experimental results obtained with several antennas at a frequency of 14 GHz.

The radiation pattern of these antennas has been measured for 14 GHz and some results are plotted in Figs. 9 and 10. The conclusion is that the experimental results are in good agreement with the theoretical predictions.

It is very interesting to investigate the effect of the length r' of the antenna on the radiation pattern. For this purpose the radiation patterns of two antennas with the same flare angle but different lengths have been given in Fig. 11. To hold the picture clear we have not plotted the theoretical patterns in Fig. 11, but the agreement is good, especially for the large antenna. We see that a large antenna has a flat radiation pattern and is very suitable as a feed in a paraboloid reflector antenna. It seems that the greatest length that can be used is not determined by electrical requirements but merely by mechanical ones, such as weight and space.

For the application of corrugated conical horn antennas it is mostly necessary that they can be used also for other frequencies than for which the grooves have a depth of a quarter of a wavelength. This question is discussed in Section 4.2.2.

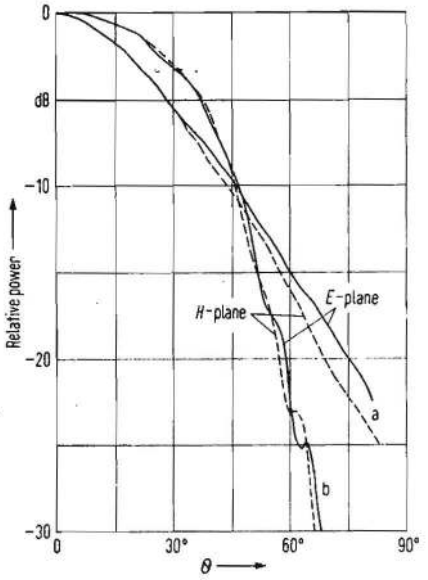

Fig. 11. Experimental radiation pattern of a large antenna and a short antenna with the same flare angle; frequency 14 GHz; a) antenna with $\theta_0 = 60°$, $r' = 2.80$ cm, b) antenna with $\theta_0 = 60°$, $r' = 13.64$ cm.

4.2.2. The bandwidth of the corrugated conical horn antenna

The bandwidths of the antennas, discussed in Section 4.2.1, have been studied by measuring the radiation pattern of each of them as a function of the frequency. The diameter of the circular waveguide, which is coupled to the cone, was so chosen that the cut-off frequency of the dominant TE_{11}-mode was approximately 10 GHz. The diameter of the waveguide is 18 mm. The depth of the grooves was a quarter of a wavelength at 14 GHz.

For conveniently constructing the antennas the depth of all the grooves was chosen equal and the boundaries of the grooves as straight lines. The purpose of the measurements which have been carried out can be formulated as follows:

i) to study surface wave phenomena, if any;
ii) to prove that a symmetrical radiation pattern is obtained if the depth of the grooves is a quarter of a wavelength. These measurements have already been discussed in the previous section;
iii) to investigate the deviation between the experimental and the theoretical results of Fig. 9 and 10, which are based on the assumption that $Z_0 H_{\varphi'}$ and $E_{\varphi'}$ are zero, independent of the frequency.

Two typical results of these measurements are plotted in Fig. 12 and 13. The solid line indicates

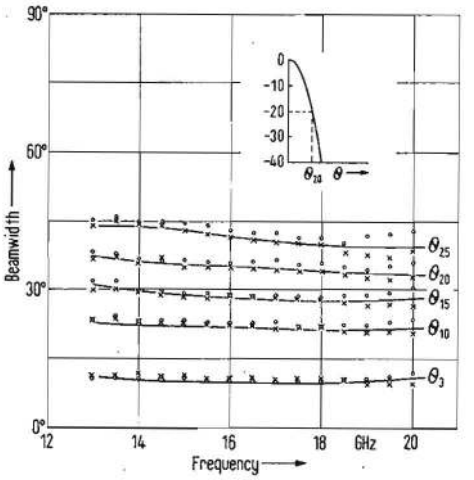

Fig. 12. Beamwidth versus frequency; antenna with $\theta_0 = 30°$ and $r' = 9.00$ cm;
— calculated, E-plane and H-plane,
o experiment, E-plane.
× experiment, H-plane.

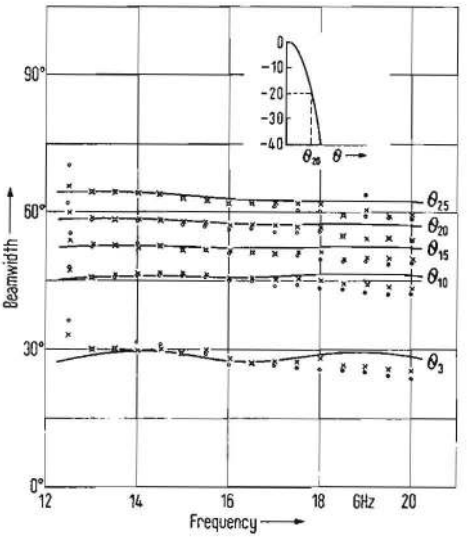

Fig. 13. Beamwidth versus frequency; antenna with $\theta_0 = 60°$ and $r' = 13.64$ cm;
— calculated, E-plane and H-plane,
o experiment, E-plane,
× experiment, H-plane.

the theoretical beamwidth, based on the assumption that $Z_0 H_{\varphi'}$ and $E_{\varphi'}$ are zero. The main conclusion is that the scalar feed is indeed a broadband feed. On closer examination we observe that for frequencies for which the depth of the grooves is smaller than a quarter of a wavelength, a sudden change occurs in the shape of the radiation pattern.

Probably this is caused by a surface wave, as discussed by KAY [16], and it is clear that for the moment this phenomenon determines the lower limit of the frequency band for which the scalar feed can be used. For frequencies between 14 GHz and 20 GHz we observe a good agreement between the experimental results and the theoretical ones represented by the solid line. Apparently we may conclude that the boundary conditions $Z_0 H_{\varphi'} = 0$ and $E_{\varphi'} = 0$ are valid in a rather large frequency range. This fact gives us the opportunity to use Figs. 9 and 10 as design charts.

We have also investigated the V.S.W.R. of the antennas as a function of the frequency. One typical example is given in Fig. 14. Unfortunately, there is a large mismatch at the frequency for which the depth of the grooves is a quarter of a wavelength. However, we have also seen that for frequencies higher than the one mentioned above good radiation patterns are obtained. So it is recommendable to choose the depth of the grooves a little larger than a quarter of a wavelength for the lowest frequency for which the antenna will be used. In that case, a good matching and a good pattern are obtained in a rather large frequency band.

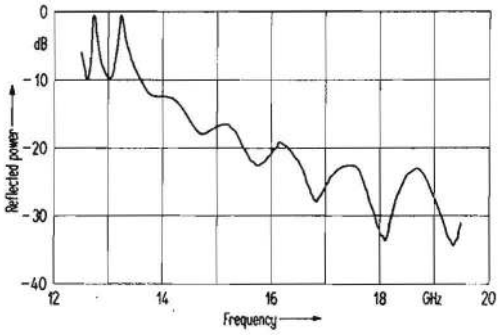

Fig. 14. Measured reflected power versus frequency; antenna with $\theta_0 = 45°$ and $r' = 3.71$ cm.

5. Conclusions

The electromagnetic field in the conical corrugated horn antenna and its radiation pattern have been studied theoretically. The main conclusion of this investigation is that the conical corrugated horn antenna has a symmetrical radiation pattern, provided the depth of the grooves is a quarter of a wavelength. The theory of the scalar feed has been formulated for this case. An experimental investigation shows that there is a good agreement between the experimental results and the theoretical calculations if the depth of the grooves is a quarter of a wavelength. Many measurements have been carried out at frequencies of 14 GHz to 20 GHz. From these measurements we can draw the following conclusions. For large antennas with a flare angle θ_0 smaller than 75° there is a good agreement between experimental results and calculations based on the assumption that $E_{\varphi'}$ and $Z_0 H_{\varphi'}$ are zero at the boundary $\theta' = \theta_0$, even at frequencies for which the depth of the grooves is not equal to a quarter of a wavelength. In case the flare angle is smaller than 75° and the antennas are short, again resonable agreement between theory and experiment has been found. The measurement of the V.S.W.R. shows that one should choose the depth of the grooves a little larger than a quarter of a wavelength for the lowest frequency for which the antenna will be used. The highest frequency which can be used is determined by the fact that the excitation of higher modes has to be prevented. An improvement of the bandwidth of the waveguide coupled to the cone will probably result in improvement of the bandwidth of the antenna.

Acknowledgements

The authors wish to thank Prof. Dr. ir. A. v. TRIER for given them the opportunity to carry out the research described in this paper. The discussions with Prof. ir. C. A. MULLER concerning the application of the scalar feed in antennas for radio-astronomical investigations are greatly appreciated. The authors appreciated the assistance of Mr. KNOBEN for the measurements carried out.

(Received July 1st, 1971.)

References

[1] SIMMONS, A. J and KAY, A. F., The scalar feed — a high performance feed for large paraboloid reflectors. Instn. Elect. Engrs. Conference Publication **21** [1966], 213–217.
[2] JEUKEN, M. E. J. and KIKKERT, J. S., A broadband aperture antenna with a narrow beam. Alta Frequenza **38** [1969], 270–276.
[3] MARCUVITZ, N., Waveguide Handbook. McGraw-Hill Book Co., New York 1951.
[4] JEUKEN, M. E. J., Experimental radiation pattern of the corrugated conical horn antenna with small flare angle. Electron. Letters **5** [1969], 484–485.
[5] CLARRICOATS, P. J. B. and SAHA, P. K., Theoretical analysis of cylincrical hybrid modes in a corrugated horn. Electron. Letters **5** [1969], 187–189.
[6] JEUKEN, M. E. J., Frequency-independence and symmetry properties of corrugated conical horn antennas with small flare angles. Ph. D. Thesis 1970, Eindhoven University of Technology, Netherlands.
[7] CLARRICOATS, P. J. B., Analysis of spherical hybrid modes in a corrugated conical horn. Electron. Letters **5** [1969], 189–190.
[8] SAHA, P. K., Propagation and radiation characteristics of corrugated waveguides. Ph. D. Thesis, University of Leeds, England, 1970.
[9] HARRINGTON, R. F., Time-harmonic electromagnetic fields; Chapter 6. McGraw-Hill Book Co., New York 1961.
[10] ABRAMOWITZ, M. and STEGUN, I. A., Handbook of mathematical functions; p. 439. Dover Publications, New York 1965.
[11] JANSEN, J. K. M., JEUKEN, M. E. J. and LAMBRECHTSE, C. W., The scalar feed. T. H. Report 70-E-12, Eindhoven University of Technology, Netherlands. (Copies of this report may be obtained on application to the second author.)
[12] ABRAMOWITZ [10], p. 336.
[13] HARRINGTON [9], p. 469.
[14] SAXON, G., JARVIS, T. R., and WHITE, I., Angular-dependent modes in circular corrugated waveguide. Proc. Instn. Elect. Engrs. **110** [1963], 1365–1373.
[15] FLÜGGE, S., Handbuch der Physik; Bd. 25, S. 238–240. Springer-Verlag, Berlin 1961.
[16] KAY, A. F., The scalar feed. TRG Report, Contract AF 19 (604)-8057, March 1964.

The following article, which appeared after the completion of the present paper, is relevant to the material presented herein:

CLARRICOATS, P. J. B. and SAHA, P. K., Propagation and radiation behaviour of corrugated feeds. Proc. Instn. Elect. Engrs. **118** [1971], 1167–1180.